Citation for published version:
Yulin, AV, Skryabin, DV & Gorbach, AV 2015, 'Dark solitons and vortices in the intrinsic bistability regime in exciton polariton condensates', Physical Review B : Condensed Matter and Materials Physics, vol. 92, no. 6, 064306. https://doi.org/10.1103/PhysRevB.92.064306

DOI:
10.1103/PhysRevB.92.064306

Publication date:
2015

Document Version
Early version, also known as pre-print

Dark solitons and vortices in the intrinsic bistability regime in exciton polariton condensates

A.V. Yulin[1], D.V. Skryabin[1,2], and A.V. Gorbach[2]
[1] *ITMO University, Kronverksky pr. 49, St. Petersburg, 197101, Russian Federation*
[2] *Department of Physics, University of Bath, Claverton Down, Bath, BA2 7AY, UK*
(Dated: August 13, 2015)

We report on a class of dark solitons and vortices existing in the exciton-polariton condensates and having discontinuity in their excitonic component. These solutions exist due to an intrinsic bistability of the exciton density in the given optical field and for non-zero detuning between the cavity and excitonic resonances. We specify a well defined energy boundary where they transform into previously known polaritonic dark solitons and vortices.

PACS numbers: 71.35.Lk 42.65.Tg

I. INTRODUCTION

Photons in optical microcavities can strongly couple to excitons and form new quasi-particles: exciton-polaritons or simply polaritons [1, 2]. These unique half-light half-matter states exhibit rich physical properties and attract great interest from condensed matter and optics communities. Inheriting a light effective mass from its photon component, microcavity polaritons demonstrate high temperature Bose-Einstein condensation [3, 4] and superfluidity [5, 6]. At the same time, due to their excitonic component, microcavity polaritons interact much stronger than photons and thus represent a competitive low-energy platform for ultrafast signal processing applications. Indeed, a range of fundamental nonlinear effects has been investigated with microcavity polaritons, including low threshold bistability [7, 8], polarization multi-stability and switching [9–11], parametric scattering and pattern formation [12–16], excitation of dark- [17–21] and bright solitons [22–28].

The existence of dark solitons is supported by the combination of the positive effective mass of polaritons with low momenta in the cavity plane, and the repulsive nonlinear interaction of polaritonic condensates. These two factors jointly ensure stability of the high amplitude background supporting dark solitons [18]. In planar systems, such as polariton microcavities, these conditions also favor formation of vortices [29]. Vortices can emerge as a result of the transverse modulational instability of dark solitons in repulsive condensates and nonlinear optical systems [21]. Spontaneous parametric scattering in resonantly driven microcavities can also lead to formation of various types of vortex-antivortex lattices [14, 30–33]. Excitation of polaritonic vortices can be triggered either by an external pulse or by the interaction with a scattering center [34]. The latter mechanism underlines similarities of polariton dynamics in microcavities with hydrodynamics of super-fluids [35]. This analogy has been further developed in the recent theoretical and experimental studies of hydrodynamical properties of vortices and dark solitons in polariton condensates [36–39].

Despite the above analogies with hydrodynamics and optics, polariton solitons and vortices have an important distinctive feature: they are inherently two-component states, and the effective masses of the photons and excitons differ by many orders of magnitude resulting in dramatically different healing lengthes. This fact is somewhat obscured, when photons and excitons are strongly coupled into polaritons that can be well described by a single order parameter function. However, as we show below, nonzero detuning between photon and exciton resonances can weaken the photon-exciton coupling to the extend that for certain energies polaritonic approach breaks down leading to new types of dark solitons and vortices having no known analogues in hydrodynamics, nonlinear optics and dynamics of atomic Bose-Einstein condensates. These solutions exists due to specific type of bistability of the system - so called *intrinsic bistability*, which refers to the situation when material polarisation is bistable in the presence of a constant applied field [40]. In our system, the intrinsic bistability manifests in multiple solutions of the excitonic wave function for a given amplitude of the intracavity photon field. We show that the intrinsic bistability provides a new and unique mechanism for localization of nonlinear excitations. Recently it was noted that polariton vortices have two distinctive characteristic lengths of localization in the photonic and excitonic components [41]. However, solutions studied in Ref. [41] can be described within the framework of the polaritonic approach and are separated from the solitons and vortices supported by the intrinsic bistability by a well defined boundary.

II. MODEL EQUATIONS

We adopt the well established dimensionless mean-field model describing dynamics of the exciton polariton condensate in an optical cavity [1, 2] in terms of coupled complex amplitudes E and ψ of the photon and exciton fields:

$$\partial_t E - i\nabla_\perp^2 E + (\gamma_1 - i\delta)E = i\psi + E_p \cdot e^{-iq_p t} \qquad (1)$$

$$\partial_t \psi - i\sigma\nabla^2\psi + (\gamma_2 + i\delta + i|\psi|^2)\psi = iE, \qquad (2)$$

where time is measured in the units of the inverse Rabi frequency $T = 1/\omega_R$, scaling of spatial coordinates L is determined by the effective cavity photon mass m_c: $L = \sqrt{\hbar/(2m_c\omega_R)}$, γ_1 and γ_2 are the attenuation coefficients for the photon and exciton fields, respectively, 2δ is the detuning between the exciton resonance and the cavity resonance, σ is the coefficient describing the diffraction of the exciton field (relative to the diffraction of photons): $\sigma = m_c/m_{ex} \sim 10^{-5}$, m_{ex} is the exciton mass, E_p and q_p are the amplitude and the detuning of the pump from the center of the gap between lower- and upper polaritonic branches. The coefficient of nonlinear interaction in the excitonic field is set to unity by the appropriate scaling of field amplitudes, see more details in Ref. [26].

III. INTRINSIC BISTABILITY AND STATIONARY SOLUTIONS

In this section we consider stationary solutions, $E = Ae^{-iqt}, \psi = \Psi e^{-iqt}$, in the limit of negligible dissipation and zero pump: $\gamma_1 = \gamma_2 = E_p = 0$. Here q is the normalised energy parameter or chemical potential. Real amplitudes A and Ψ solve the following set of equations:

$$\left(\partial_x^2 + \partial_y^2\right) A + (q+\delta)A + \Psi = 0 \ , \tag{3}$$

$$\sigma(\partial_x^2 + \partial_y^2)\Psi + (q - \delta - \Psi^2)\Psi + A = 0 \ . \tag{4}$$

Neglecting nonlinearity, the spectrum of the linear zero momentum polaritons $E, \psi \sim e^{-iqt}$ is given by

$$q = \pm\sqrt{1+\delta^2} \ . \tag{5}$$

This defines the energy gap between the lower and upper polariton branches, see Fig. 1.

Eqs. (3, 4) have three spatially independent (homogeneous) solutions: one is the trivial $A = \Psi = 0$ and the other two are the nontrivial ones $A(x,y) = A_h$, $\Psi(x,y) = \Psi_h$ differing by the phase change by π:

$$A_h = \frac{\pm|\Psi_h|}{|q+\delta|} \ , \qquad \Psi_h = \pm\sqrt{\frac{q^2-\delta^2-1}{q+\delta}}. \tag{6}$$

Since Ψ_h is assumed real, the above solution exists either for $-\sqrt{1+\delta^2} < q < -\delta$ or for $q > \sqrt{1+\delta^2}$. However this solution is modulationally stable, i.e. stable with respect to the spontaneous parametric generation, only in the domain touching the lower polariton branch. This domain is shaded in green and black colors in Fig. 1. All the discussion and results presented below are related only to the region where the homogeneous solution is modulationally stable, since the absence of the spontaneous instabilities of the background is essential for experimental observation of the dark solitons and vortices.

Neglecting the kinetic energy term in the excitonic field, $\sigma = 0$, Eq. (4) becomes the cubic algebraic equation:

$$(q-\delta)\Psi - \Psi^3 + A = 0 \ . \tag{7}$$

Eq. (7) is guaranteed to have only one real solution for any A providing $q < \delta$. However, for $q > \delta$, Eq. (7) can have either one or three real roots depending on the value of A. The latter situation corresponds to the intrinsic bistability of the excitonic system. The range of parameters where the intrinsic bistability coexists with the stable homogeneous solution is shaded in green in Fig. 1. Thus, for a given amplitude A of the photonic component, Eq. (7) admits either one or three real solutions: $\Psi = \Psi_m(A)$, $m = 1,2,3$. Note, that $\delta = 0$ in Ref. [41], which excludes the intrinsic bistability near the lower polariton branch from consideration.

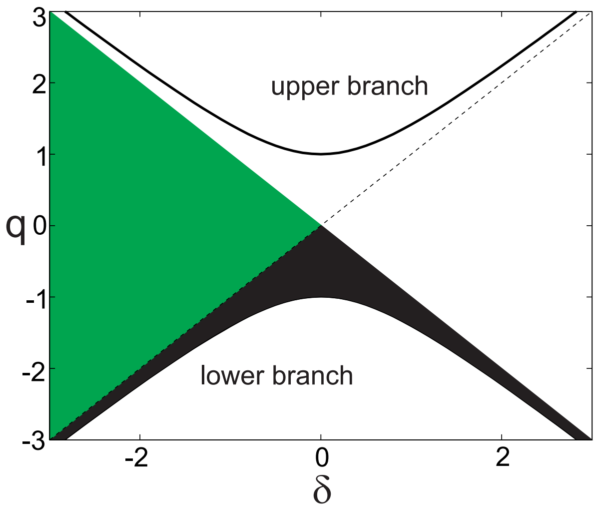

FIG. 1: (Color online) Domains shaded in green and black is the existence domain of the spatially homogeneous and modulationally stable background. The green part corresponds to the parameters where a stable background coexists with the intrinsic bitsability and the black one is where it does not.

To describe localized solutions, we now consider spatially nonuniform amplitudes A and Ψ and assume $\sigma = 0$. With the account of three possible solutions, Ψ_m, of the algebraic equation (7), Eqs. (3, 4) can be written as the three simultaneous equation for the photonic amplitude A:

$$(\partial_x^2 + \partial_y^2)A + (q+\delta)A + \Psi_m(A) = 0 \ , \quad m = 1,2,3 \ . \tag{8}$$

Let us first discuss the 1D case in which the fields are y independent. Then, Eq. (8) is equivalent to the equation describing dynamics of a particle in a potential:

$$\partial_x^2 A = -\frac{\partial F_m}{\partial A} \ , \tag{9}$$

$$F_m(A) = \frac{3\Psi_m^4(A)}{4} - \frac{(q-\delta)\Psi_m^2(A)}{2} + \frac{(q+\delta)A^2}{2} \ . \tag{10}$$

In the derivation of Eq. (10) we used $\partial F_m/\partial A = \partial F_m/\partial\Psi_m \cdot (\partial A/\partial\Psi_m)^{-1}$, where $\partial A/\partial\Psi_m$ is obtained by the direct differentiation of Eq. (7). The potentials $F_m(A)$ for the parameters inside the the green area in Fig. 1 are shown in the top two panels of Fig. 2 (the intrinsic bistability case). The single potential existing in the black area, i.e. outside the intrinsic bistability range, is shown in the bottom panel. Maxima or minima of these potentials corresponds to the stationary homogeneous solution of our system. In general, in the intrinsic bistability case, when the three potentials coexist over the interval of A around zero, $|A|^2 < (q-\delta)/3/(q+\delta)^2$, the two nontrivial homogeneous solutions (6), can either belong to the two different potentials $F_{2,3}$, as in the top panels in Fig. 2, or to the potential F_1. The latter situation can exist only outside the stability domain of the homogeneous solution and therefore is not shown here. The trivial solution in all the cases belongs to the F_1 potential. As parameters cross the border $q = \delta$ of the intrinsic bistability range, the potential changes its shape from the one with cusps (inside the intrinsic bistability range) to the smooth one, as illustrated in Fig. 2.

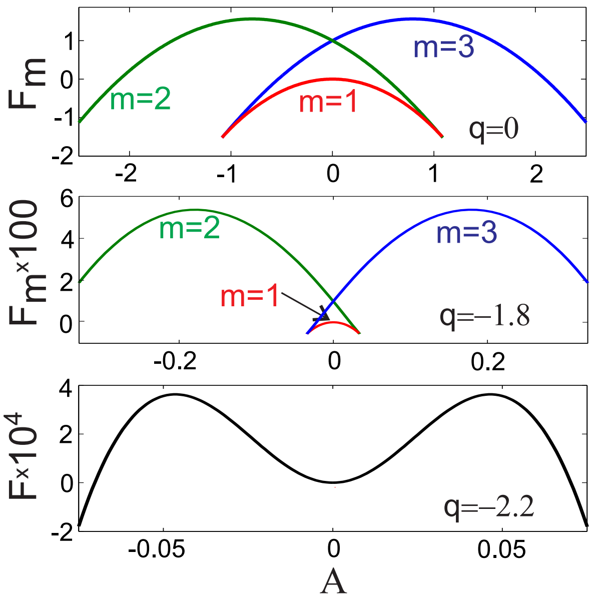

FIG. 2: (Color online) Potential functions F_m, Eq. (10), for the intrinsic bistability ($q = 0$, $q = -1.8$) and no intrinsic bistability ($q = -2.2$) cases. The detuning is fixed to $\delta = -2$.

Conventional dark solitons are the heteroclinic trajectories connecting two saddle points of the potential in the bottom panel of Fig. 2 and crossing the point $A = 0$ in an obvious way. There are two possible ways for a similar heteroclinic connection to exist for the potentials in the two top panels. First, is when the trajectory jumps straight from the branch $m = 2$ to $m = 3$ at $A = 0$, i.e. at the only point where F_2 crosses with F_3. The phase planes and the resulting solution corresponding to this case are shown in the left column of Fig. 3. Ψ-field undergoes a discontinuous jump at the soliton core, which is mathematically allowed, since the equation for Ψ is algebraic. At the same point, continuity of the A field and its derivative $\partial_x A$ is preserved, since the phase trajectories intersect if the phase planes are overlapped. The second possible case, is when the trajectory switches from the branch $m = 2$ to $m = 1$, crosses $A = 0$ while on $m = 1$, and then jumps to $m = 3$, see the right column in Fig. 3. Switching to and from the $m = 1$ branch can happen for the values of A, where $F_1 < 0$, so that there is always a required intersection of the phase trajectories to keep both A and its derivative continuous. In this case the distance along x between the two discontinuities can be varied as a soliton parameter.

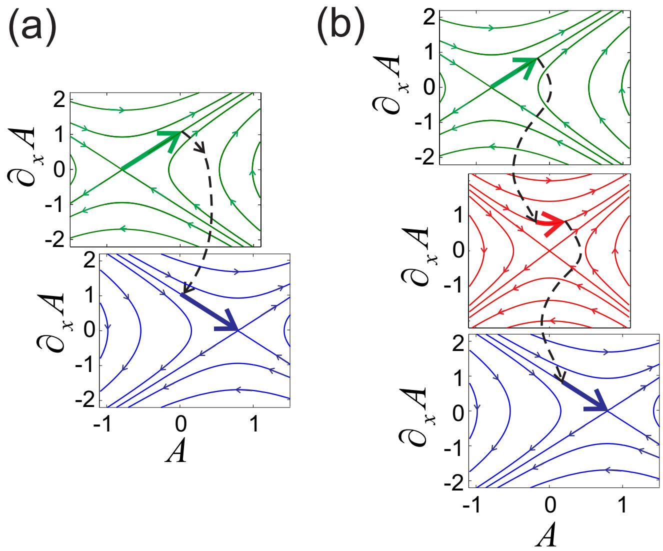

FIG. 3: (Color online) The phase planes for the potentials $F_{2,3}$ (a) and for $F_{1,2,3}$ (b): $q = 0$, $\delta = -2$. Bold full and dashed lines show possible heteroclinic connections and jumps between the different potentials corresponding to the dark solitons with one (a) or two (b) discontinuities.

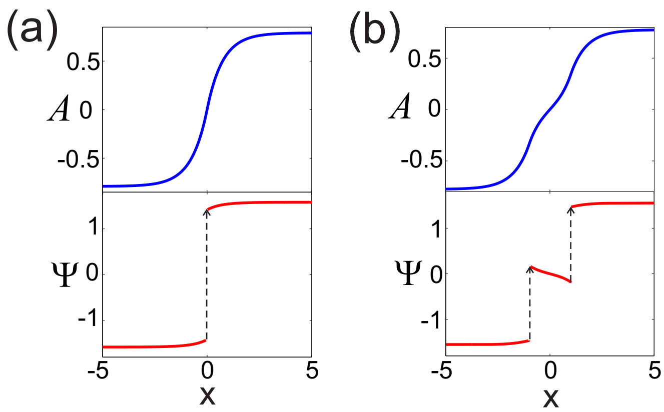

FIG. 4: (Color online) The soliton solutions corresponding to the phase trajectories shown in Fig. 3

Note, that, for the soliton with $\Psi(x)$ discontinuous at

$x = 0$, the $|\Psi|$ is continuous and has the different from zero minimum at $x = 0$, see Fig. 5(a). Approaching the intrinsic instability boundary $q = \delta$ from above, i.e. by reducing q, the soliton background and the minimum of $|\Psi|$ decrease, see Fig. 5(b). At the point $q = \delta$, the minimum of $|\Psi|$ hits zero, for $q < \delta$ the intrinsic bistability cease to exist and the dark solitons with discontinuities transform into the conventional ones for which the minimum of $|\Psi|$ stays at zero. The boundary of the range of the energy parameter q, where the novel type of dark solitons exists is detuned from the lower polariton energy by $\sqrt{1+\delta^2} - |\delta|$ (for $q, \delta < 0$) and spreads all the way towards the energy corresponding to the upper polariton branch, see Figs. 5(b) and 1.

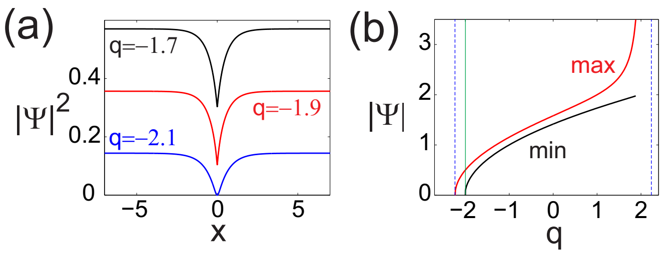

FIG. 5: (Color online) Transition from the intrinsic bistability dark solitons to the conventional ones. (a) shows the excitonic density profiles of the dark solitons with discontinuities at $x = 0$ (q=-1.7, q=-1.9) and of the conventional one ($q = -2.1$): $\sigma = 0$. (b) shows how the background excitonic density ($max|\psi|$, red solid line) and the density at the center of the dark soliton ($max|\psi|$, black dashed line) vary with the energy parameter q for $\delta = -2$. The transition between the two types of solitons happens at $q = \delta$. The dashed vertical lines mark the q values at the lower and upper polariton branches. Full vertical line marks the intrinsic bistability boundary.

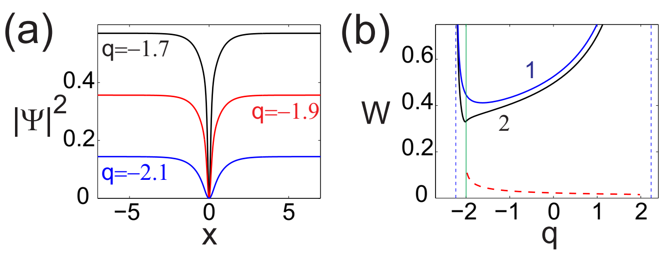

FIG. 6: (Color online) (a) Exciton density profiles for the dark soliton solutions. Parameters are the same as in Fig. 5(a), but $\sigma = 0.0025$. (b) Line 1 is the width of the photonic core for the dark soliton solutions across the full range of the soliton existence. Line 2 is the width of the broad part of the excitonic density in the soliton core. The dashed red line shows the width of the narrow part of the excitonic density in the soliton core. The dashed vertical lines mark the q values at the lower and upper polariton branches. Full vertical line marks the intrinsic bistability boundary.

Restoring the kinetic energy term in the equation for Ψ, and using that $\sigma << 1$, one can assume that $A = 0$ around the excitonic core in the leading order approximation and hence recover the Gross-Pitaevskii equation for Ψ only. For the dark solitons in this model the density drops all the way to zero at the soliton core and the core size scales as $\sqrt{\sigma} << 1$. In order to confirm that this is indeed the case we have found the soliton profiles with $\sigma \neq 0$ numerically, see Fig. 6(a). Comparing the latter with Fig. 5(a) one can see that the dark soliton core now have two spatial scales. The large one is determined by the polaritonic healing length, which is ~ 1, and the small one is by the excitonic healing length $\sim \sqrt{\sigma}$. The transition between the two happens at the $|\Psi|$ value close to the one corresponding to the discontinuity of Ψ in the $\sigma = 0$ case.

The dependencies of the widths of the photonic core and of the large scale part of the excitonic core on the energy parameter q are shown in Fig. 6(b) with the full lines. One can see that these two widths are approximately the same inside and outside the intrinsic bistability range. The dashed line shows the much smaller width of the additional deep developing in the excitonic component inside the intrinsic bistability range. Photonic and excitonic components of the dark soliton in the intrinsic bistability range and for $\sigma \neq 0$ are shown for comparison in Fig. 7(a). Thus the main physical signature of a new type of dark solitons should be sought through the direct or indirect measurements of the excitonic density, which will require development of new experimental techniques, since the existing ones focus on the photonic part of the polaritonic field.

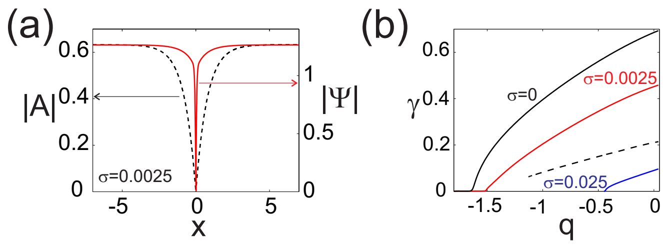

FIG. 7: (Color online) (a) Photonic and excitonic components of the intrinsic bistability dark solitons with $\sigma \neq 0$. The other parameters are: $\delta = 1.55$, $q = -0.45$. (b) The dark soliton instability growth rate (full lines) as a function of q for $\sigma = 0.25, 0.025, 0.0025$, and the same for the soliton with two discontinuities separated by a distance 1, $\sigma = 0$ (dashed curve).

The intrinsic bistability dark solitons with discontinuities can be generalized to two dimensional vortices. Introducing polar coordinates (r, θ), and looking for radially symmetric solutions in the form $A = f(r)\exp(im\theta)$, $\Psi = p(r)\exp(im\theta)$, where m is the topological charge of the vortex, it is easy to write the analogue of Eq. (8) for the functions $f(r)$ and $p(r)$. Numerical solutions of this equation corresponding to the vortices ($m = 1$) localized

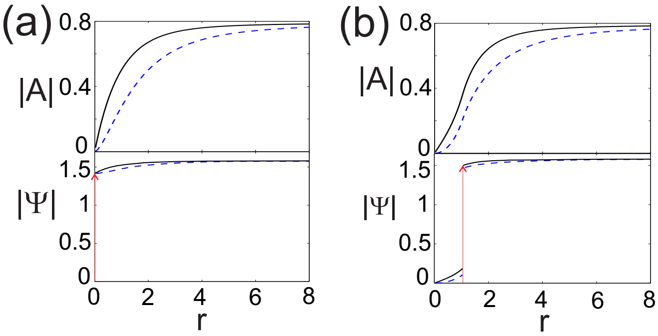

FIG. 8: (Color online) Radial profiles of intrinsic bistability vortices with $m = 1$ (solid curves) and $m = 2$ (dashed curves). In panel (a) vortex solitons with the discontinuity in Ψ field in the centre ($r = 0$) are shown. The vortex solitons in panel (b) have discontinuity along the ring ($r = 1$). The parameters are $\sigma = 0$, $q = 0$, $\delta = -2$.

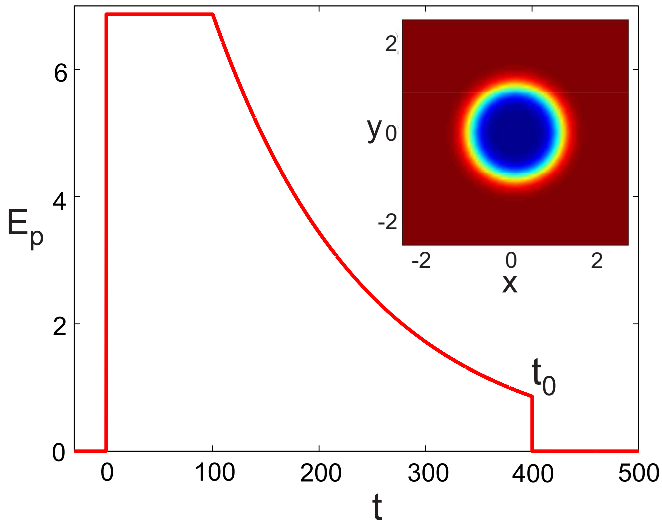

FIG. 9: (Color online) The variation of the pump amplitude $E_{p0}(t)$ in the numerical experiment. The inset shows the spatial distribution of the intensity of the pump.

at discontinuities in Ψ field are shown in Fig. 8.

IV. STABILITY ANALYSIS AND DYNAMICAL EVOLUTION

To observe dark solitons and vortices in experiments, the solutions must also be dynamically stable. We have studied the stability of the solitons by solving the corresponding spectral problem and by direct numerical simulation of Eqs. (1)-(2) with the noise added to the soliton profiles. The dependencies of the instability growth rates on the soliton parameter q are shown in panel (d) of Fig. 7 for different values of σ.

The linear stability analysis of the conventional dark solitons reveals that they become unstable with respect to the drift instability when q is increasing and is approaching $q = \delta$ boundary of the intrinsic bistability. The same instability is inherited by the dark solitons with discontinuities. Increasing dispersion in the exciton model tends to suppress this instability, see Fig. 7(d). Due to weakness of the above instability we are expecting that it should not prevent observations of the solitons and vortices in the experiments where polaritons have a finite life time of ~ 10 ps. We performed numerical simulations of the 2D polariton system excited by a vortex beam and observed the intrinsic bistability vortices. The instability growth rate appears to be further suppressed by the dissipation and the observation time limited by the lifetime of polaritons is sufficient for the soliton observation.

In our numerical experiment we have excited the system by an optical vortex beam with the topological charge one:

$$E_p = E_{p0}(t) \times \times \left[2 + \tanh\left(\frac{r - r_0}{w_p}\right) - \tanh\left(\frac{r + r_0}{w_p}\right)\right] \frac{x + iy}{2r},$$

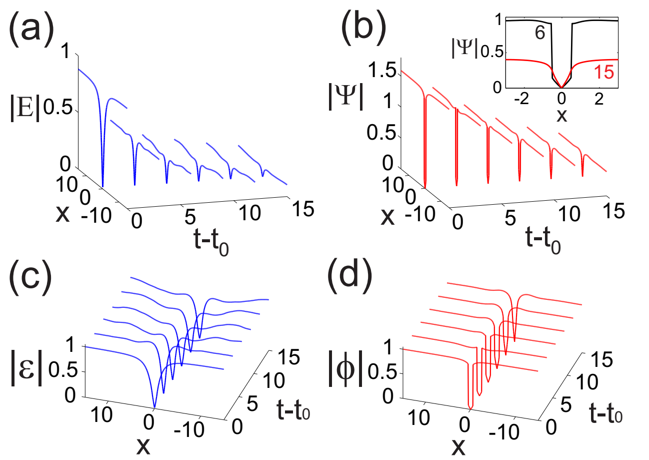

FIG. 10: (Color online) Field evolution in the numerical experiment: fields E and Ψ, panels (a) and (b), and renormalized fields $\varepsilon = |E|/\max\,|E|$ and $\Phi = |\Psi|/\max\,|\Psi|$, panels (c) and (d). Parameter values are: $\sigma = 0$, $q_p = 0$, $\delta = -2$, $\gamma_1 = \gamma_2 = 0.1$. The inset in panel (b) shows profiles of $|\Psi|$ field at $t - t_0 = 6$ and $t - t_0 = 15$, the curves are marked correspondingly.

where $r = \sqrt{x^2 + y^2}$, and we chose $r_0 = 1$, $w_p = 0.25$. The corresponding spatial profile of the pump intensity is shown in the inset of Fig. 9. The pump frequency was set to $q_p = 0$. We switched the pump on at $t = 0$ and took the initial amplitude large enough to create high polariton density in the vortex background, which subsequently decayed through the losses towards its stationary value. At $t = 100$ we started to decrease adiabatically the pump until at $t_0 = 400$ it reached the value $E_{p0} = 0.43$, see Fig. 9, bringing the values of E and Ψ close to the solution (6). Then we switched the pump off, which has led to the formation of the intrinsic bistability vortex, see Fig. 10. The structure of the vortex is better seen in the re-normalised representation, see Fig. 10 (c), (d).

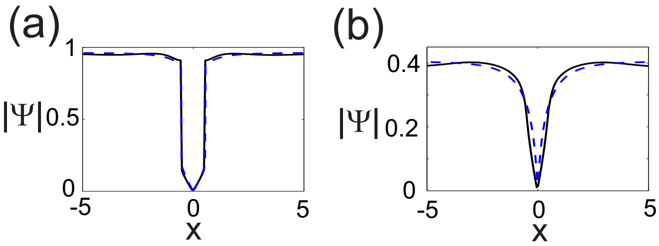

FIG. 11: (Color online) Field profiles in the numerical experiment for the times $t - t_0 = 6$ (a) and $t - t_0 = 15$ (b). Dashed curves show the stationary vortex solution for the conservative problem.

Initially, the vortex core in Ψ has discontinuity at a certain distance from the center, see Figs. 10(b,d). With the decay of the background the q-parameter slides down towards $q = \delta$ boundary and at some time moment these discontinuities disappear and the usual continuous vortex is emerging. Further examples of the transverse profiles of the discontinuous vortex at $t - t_0 = 6$ and of the continuous one at $t - t_0 = 15$ are shown in Fig. 11, where they are also compared with the exact solutions.

V. CONCLUSION

We have demonstrated that the intrinsic bistability of excitons leads to the existence of a new type of dark solitons and vortices. Without dispersion of the exciton field these structures have discontinuities in the exciton field. Adding small, but non-zero dispersion in the excitonic field removes these discontinuities and results in dark solitons and vortices, which have very different core sizes in the optical and excitonic fields. This class of vortices and solitons exists for the exciton densities higher than required for the previously studied ones, that can be well described by the polaritonic order parameter and have comparable core sizes in the excitonic and optical components [41]. The densities required are however, very realistic, since they should merely lead to the upwards polariton energy shifts exceeding the energy offset between the excitonic and cavity resonances by any amount. We have also shown that the formation of the intrinsic bistability vortices in the decaying condensate under the realistic excitation conditions takes place despite dynamical instabilities having characteristic time larger than the typical life time of the polariton condensate.

Acknowledgements

AVY and DVS acknowledge support from the Government of the Russian Federation (Grant 074-U01) through the ITMO University early career fellowship and visiting professorship schemes. All authors acknowledge financial support from the EU network project LIMACONA (Project No: 612600). DVS and AVG acknowledge funding through Leverhulme Trust Research Project Grant RPG-2012-481.

[1] A. V. Kavokin, J.J. Baumberg, G. Malpuech, and F.P. Laussy, *Microcavities* (Oxford University Press, Oxford, 2007).
[2] *Exciton Polaritons in Microcavities* , edited by D. Sanvitto and V. Timofeev, Springer Series in Solid-State Sciences Vol. 172(Springer, Heidelberg, 2012).
[3] J. Kasprzak *et al.*, Nature Physics **443**, 409 (2006).
[4] R. Balili, V. Hartwell, D. Snoke, L. Pfeiffer, and K. West, Science **316**, 1007 (2007).
[5] I. Carusotto and C. Ciuti, Phys. Rev. Lett. **93**, 166401 (2004).
[6] A. Amo et al., Nature Phys. **5**, 805 (2009).
[7] A. Baas, J. Karr, H. Eleuch, and E. Giacobino, Phys. Rev. A **69**, 023809 (2004).
[8] N. A. Gippius, S. G. Tikhodeev, V. D. Kulakovskii, D. N. Krizhanovskii, and A. I. Tartakovskii, Europhys. Lett. **67**, 997 (2004).
[9] D. Sarkar *et al.*, Phys. Rev. Lett. **105**, 216402 (2010).
[10] A. Amo *et al.*, Nature Photon. **4**, 361 (2010).
[11] T. K. Paraiso, M. Wouters, Y. Leger, F. Morier-Genoud, and B. Deveaud-Pledran, Nature Mater. **9**, 655 (2010).
[12] P. G. Savvidis *et al.* Phys. Rev. Lett. **84**, 1547 (2000).
[13] M. Wouters and I. Carusotto, Phys. Rev. B **75**, 075332 (2007).
[14] A. V. Gorbach, R. Hartley, and D. V. Skryabin, Phys. Rev. Lett. **104**, 213903 (2010).
[15] H. Saito, T. Aioi, and T. Kadokura, Phys. Rev. Lett. **110**, 026401 (2013).
[16] M.H. Luk, Y.C. Tse, N.H. Kwong, P.T. Leung, P. Lewandowski, R. Binder, and S. Schumacher, Phys. Rev. B **87**, 205307 (2013)
[17] A. Amo, S. Pigeon, D. Sanvitto, V.G. Sala, R. Hivet, I. Carusotto, F. Pisanello, G. Lemenarger, R. Houdre, E. Giacobino, C. Ciuti, and A. Bramati, Science **332**, 1167 (2011).
[18] A. V. Yulin, O. A. Egorov, F. Lederer, and D. V. Skryabin, Phys. Rev. A **78**, 061801(R) (2008).
[19] A. Werner, O.A. Egorov, and F. Lederer, Phys. Rev. B

85, 115315 (2012).
[20] F. Pinsker and H. Flayac, Phys. Rev. Lett. 112, 140405 (2014).
[21] L.A. Smirnov, D.A. Smirnova, E.A. Ostrovskaya, and Yu.S. Kivshar, Phys. Rev. B **89**, 235310 (2014).
[22] O. A. Egorov, D. V. Skryabin, A. V. Yulin, and F. Lederer, Phys. Rev. Lett. **102**, 153904 (2009).
[23] O. A. Egorov, D. V. Skryabin, and F. Lederer, Phys. Rev. B **82**, 165326 (2010).
[24] O. A. Egorov, D. V. Skryabin, and F. Lederer, Phys. Rev. B, **84**, 165305 (2011).
[25] O. A. Egorov, D. V. Skryabin, and F. Lederer, in *Theory of Polariton Solitons*, edited by Z. Chen and R. Morandotti, Springer Series in Optical Sciences Vol. 170 (Springer,New York/Heidelberg, 2012), p. 171.
[26] M. Sich, D. N. Krizhanovskii, M. S. Skolnick, A. V. Gorbach, R. Hartley, D. V. Skryabin, E. A. Cerda-Mendez, K. Biermann, R. Hey, and P. V. Santos, Nat. Photon. **6**, 50 (2012).
[27] O. A. Egorov and F. Lederer, Phys. Rev. B **87**, 115315 (2013).
[28] M. Sich, F. Fras, J.K. Chana, M.S. Skolnick, D.N. Krizhanovskii, A.V. Gorbach, R. Hartley, D.V. Skryabin, S.S. Gavrilov, E.A. Cerda-Mndez, K. Biermann, R. Hey, and P.V. Santos, Phys. Rev. Lett. **112**, 046403 (2014)
[29] E.A. Ostrovskaya, J. Abdullaev, A.S. Desyatnikov, M.D. Fraser, and Yu.S. Kivshar, Phys. Rev. A 86, 013636 (2012).
[30] J. Keeling and N.G. Berloff, Phys. Rev. Lett. 100, 250401 (2008).
[31] F. M. Marchetti, M. H. Szymanska, C. Tejedor, and D. M. Whittaker, Phys. Rev. Lett. 105, 063902 (2010).
[32] M.O. Borgh, G. Franchetti, J. Keeling, and N.G. Berloff, Phys. Rev. B 86, 035307 (2012).
[33] F. Manni, T. C. H. Liew, K. G. Lagoudakis, C. Ouellet-Plamondon, R. Andr, V. Savona, and B. Deveaud, Phys. Rev. B 88, 201303(R) (2013).
[34] T.C.H. Liew, Yuri G. Rubo, and A.V. Kavokin, Phys. Rev. Lett. 101, 187401 (2008).
[35] D R Tilley and J Tilley, Superfluidity and Superconductivity(IOP publishing Ltd., Bristol, 1990)
[36] S. Pigeon, I. Carusotto, and C. Ciuti, Phys. Rev. B 83, 144513 (2011).
[37] G. Grosso, G. Nardin, F. Morier-Genoud, Y. Lger, and B. Deveaud-Pldran, Phys. Rev. Lett. 107, 245301 (2011).
[38] G. Grosso, G. Nardin, F. Morier-Genoud, Y. Leger, and B. Deveaud-Pledran, Phys. Rev. B 86, 020509(R) (2012).
[39] Hiroki Saito, Tomohiko Aioi, and Tsuyoshi Kadokura, Phys. Rev. B 86, 014504 (2012)
[40] J.A. Goldstone and E. Garmire, Phys. Rev. Lett. **53**, 910 (1984).
[41] N.S. Voronova, Yu.E. Lozovik, Phys. Rev. B **86**, 195305 (2012).
[42] M. Tinkham, Introduction to Superconductivity, (McGraw-Hill Book Co., Singapore, 1996).